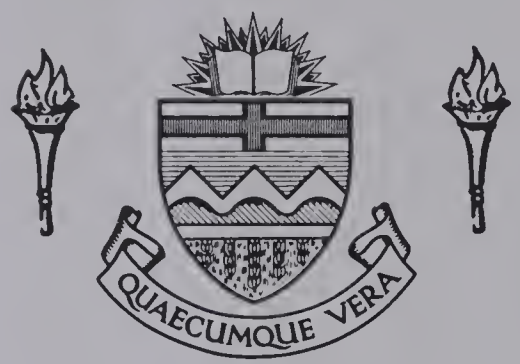

THE UNIVERSITY OF ALBERTA

RELEASE FORM

NAME OF AUTHOR: James William Pasos

TITLE OF THESIS: Small angle scattering on ^{40}Ca

DEGREE FOR WHICH THESIS WAS PRESENTED: Master of Science

YEAR THIS DEGREE GRANTED: 1975

THE UNIVERSITY OF ALBERTA

SMALL ANGLE SCATTERING ON ^{40}Ca

by

© JAMES WILLIAM PASOS

A THESIS

SUBMITTED TO THE FACULTY OF GRADUATE STUDIES AND RESEARCH

IN PARTIAL FULFILLMENT OF THE REQUIREMENTS FOR THE DEGREE

OF MASTER OF SCIENCE

DEPARTMENT OF PHYSICS

EDMONTON, ALBERTA

FALL, 1975

THE UNIVERSITY OF ALBERTA

FACULTY OF GRADUATE STUDIES AND RESEARCH

The undersigned certify that they have read, and recommend to the Faculty of Graduate Studies and Research, for acceptance, a thesis entitled SMALL ANGLE SCATTERING ON ^{40}Ca submitted by James William Pasos in partial fulfillment of the requirements for the degree of Master of Science.

ABSTRACT

The elastic scattering of 5.0 MeV deuterons incident on ^{40}Ca was measured for the forward angles. The purpose of the measurements was to test the sensitivity of the optical model parameters, particularly to small deviations from Rutherford scattering. The problems of separating the other predominant elastic peaks, ^{16}O and ^{12}C contaminants from ^{40}Ca was encountered. Large deviations from the Rutherford scattering cross-section for both these nuclei were attributed to an appreciable nuclear part of the scattering amplitude predicted by the optical model.

ACKNOWLEDGEMENTS

My supervisor, Gerry Roy, not only suggested the project but also assisted in the preliminary experimental investigation. I would like to express my appreciation for his contributions to the thesis and my education.

I would like to thank Doug Sheppard for his encouragement and continuous support.

I am very grateful to Helmy Sherif for his theoretical discussions that have considerably added to my understanding of nuclear physics.

Croy C. Neilson, Ken Dawson, Jack T. Sample, John Cameron, Gerry Moss, Bill Olsen, John McDonald and Glen Stinson also made valuable contributions to my education over the past years at one time or the other.

Many thanks to Dave Hutcheon, Dave Gill, S. T. Lam, Terry Taylor and Harry Fielding for their valuable comments.

I wish to express my gratitude to my colleagues; Bill Saunders, Sayed Elbakr, Ed Wong, Peter Green, Paul Gutowski, Aadu Hussein, Titak Sharma, Woon Chung, Jan Soukup, Dave White, Bob McCamis and Peter Johnson, who all helped in more ways than I could ask.

A special thanks goes to Jim Easton for his advice in computer programming and showing me what computers can really do.

Thanks are extended to "Uncle Jock" Elliott, Lars Holm, Paul Karvonen, Ron Popik, Don Presckarchuk, John Schaapman and John Ritzel for their technical assistance.

Thanks also goes to the secretarial staff: Gretta Tratt, Audrey Schaapman, Marie Proverb, Beth Kenyon and Maggie Fisher for their assistance and to Mrs. Helen Hawkes, who looks after us poor graduate students.

Finally, my sincere gratitude to Lee Cech for the final typing of the manuscript in spite of many last minute changes.

TABLE OF CONTENTS

LIST OF TABLES

LIST OF FIGURES

CHAPTER 1

INTRODUCTION

The purpose of the thesis is to report measurements of the absolute cross-sections in the forward-angle region between 7 to 30 degrees for deuterons scattered from calcium at 5.0 MeV and to discuss the results of the oscillatory deviations predicted in the optical-model calculations. The investigation was carried out because of the interest in the deuteron-nucleus interaction, particularly since little experimental information is available for the forward angles. The thesis attempts to resolve some of the difficulties and suggest comments or solutions for parts of the experiment not completed.

Angular distributions of 5.0 MeV deuterons scattered from ^{12}C, ^{16}O and ^{40}Ca nuclei were measured between 7 to 160 degrees. At low beam energies, say 5.0 MeV, one would expect scattering from the above nuclei to be pure Coulomb in the forward angles. However, the forward-scattering amplitude contains not only a Coulomb part but also nuclear contributions. As the scattering angle approaches zero degrees, the centre of mass of the elastic peaks shift with angle: ^{12}C shifts into ^{16}O while both peaks move into ^{40}Ca [Fig. 1.1]. One cannot subtract the ^{12}C and ^{16}O peaks from ^{40}Ca without taking into account the appreciable nuclear part.

For incident-proton energies of 2.5, 3.0 and 3.5 MeV, angular distributions were obtained for ratios between relative and absolute cross sections. Unfortunately, the cross sections for the elastic scattering of low-energy protons from ^{12}C and ^{16}O nuclei deviate from Rutherford scattering.

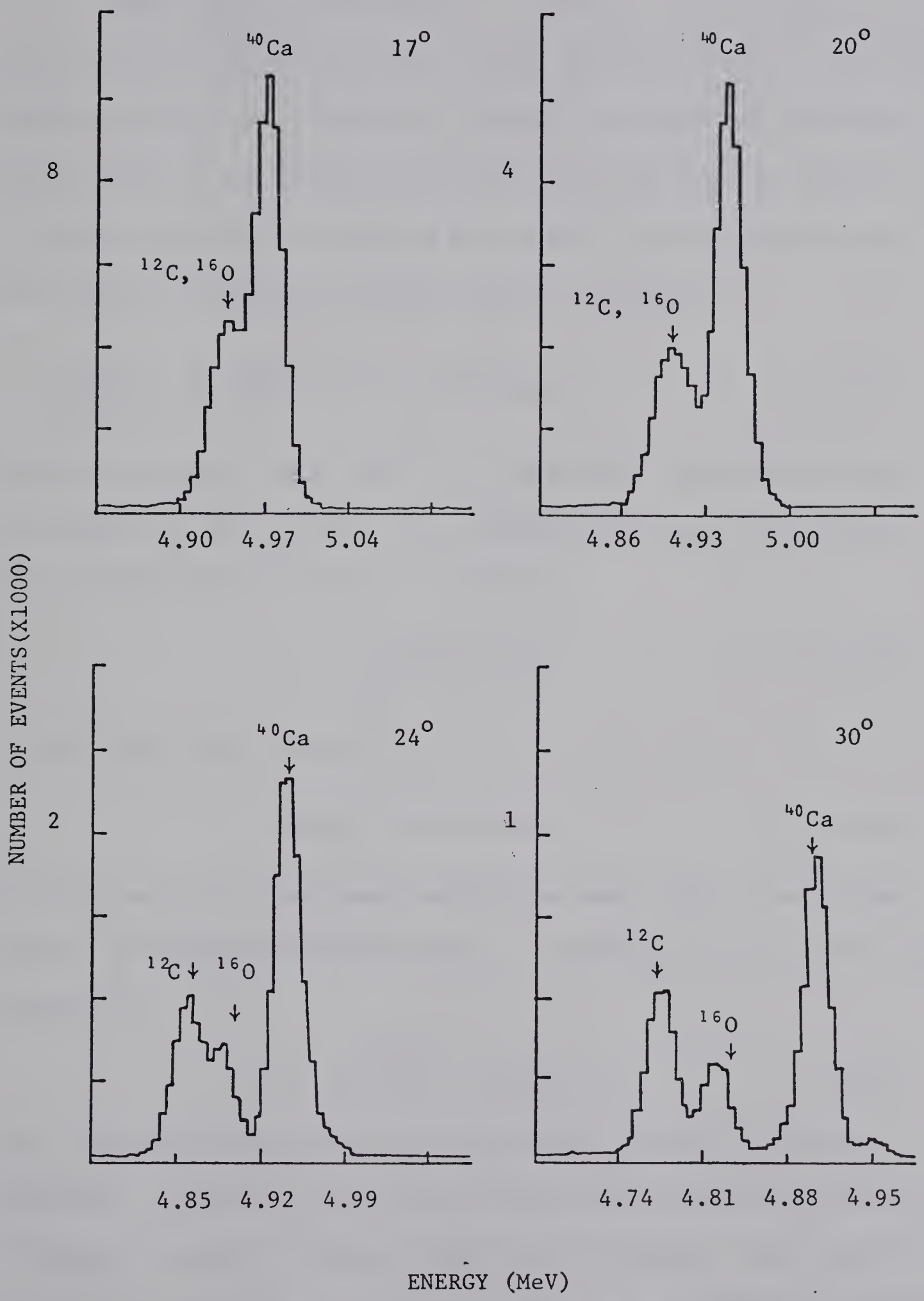

Figure 1.1 Elastic Peaks at 17, 20, 24 and 30 degrees for 5.0 MeV deuterons.

CHAPTER 2

THEORY

2.1 Rutherford Scattering

When incident particles are scattered from a target nucleus, the interaction may be described in terms of their charges. Unless the incident particles have sufficient energy to overcome the repulsive Coulomb force of the nucleus, they cannot approach closely enough to the target nucleus to be affected by the short-range nuclear force. The nonrelativistic Rutherford scattering cross section is

$$\frac{d\sigma(\theta)}{d\Omega(\theta,\phi)} = \frac{1}{4}\left(\frac{z_p z_t e^2}{2E}\right) \csc^4(\theta/2) \text{ mb/sr} \qquad (2.1\text{-}1)$$

The scattering angle is θ while E is the incident laboratory energy. The charges $z_p e$ and $z_t e$ are of the particle and target respectively. Since the scattering into ϕ is isotropic

$$\int_o^{2\pi} d\phi = 2\pi \qquad (2.1\text{-}2)$$

then the solid angle reduces to

$$d\Omega(\theta,\phi) = 2\pi \sin\theta \, d\theta \qquad (2.1\text{-}3)$$

The above expression increases rapidly for small angle θ and becomes infinite as θ approaches zero degrees. Rewriting in terms of the impact parameter b,

$$db = -\left(\frac{z_p z_t e^2}{4E}\right) \csc^2(\theta/2) \, d\theta \qquad (2.1\text{-}4)$$

shows that small-angle scattering corresponds to very large impact parameters. Therefore, the nuclear contributions should get smaller as the impact parameter b becomes larger and the Coulomb force predominates. Angular distributions may be plotted as the ratio $(d\sigma(\theta)/d\Omega)_{Exp}/(d\sigma(\theta)/d\Omega)_{Ruth}$ which effectively divide out the Coulomb effects and show graphically only the nuclear part.

2.2 Optical Model

From charged particle data, the optical model (H071) is a useful description of the elastic-scattering results, and the aim is to find smooth trends in the potential parameters as a function of mass number and energy. The optical model used is defined by the sum of the following potentials:

i) Coulomb potential

$$\frac{Zp Z_t e^2}{2R_c}\,[3-(r/R_c)^2] \qquad \text{for } r \leq R_c$$

$$\frac{Zp Z_t e^2}{r} \qquad \text{for } r \geq R_c$$

$$R_c = r_c A^{1/3}$$

The Coulomb potential, V_c would be that produced by a uniform charge distribution of classical radius, R_c. Since the experimental results are not sensitive to the value of R_c, throughout the analysis, R_c is fixed at $R_c = 1.3\ A^{1/3}$ where A is the mass number of the target nucleus.

ii) Central potential,

real part $\qquad -Vf(x_o)$

imaginary part $\qquad -W_s f(x_w) - 4a_w W_D df(x_w)/dr$

The function $f(x_i)$ is the usual Woods-Saxon form factor, $f(x_i) = [1 + \exp(x_i)]^{-1}$ where $x_i = (r-r_i A^{1/3})/a_i$ with the appropriate radius and diffuseness geometrical parameters, (r_o, a_o, r_w, a_w, r_{so}, and a_{so}). The imaginary potential is composed of a volume part W_s, (set

equal to zero in the present work) and a surface part W_D. The factor 4 appearing is required so that the surface form factor is a maximum when

$$4a_w \, df(x_w)/dr/x_w = 1$$

iii) Spin-orbit potential

$$(\hbar/m_\pi c)V_{so} \; (1/r) \; df(x_{so})/dr \; \underset{\sim}{L}\cdot\underset{\sim}{\sigma}$$

where $(\hbar/m_\pi c)^2 = 2$ fm^2. The operator $\underset{\sim}{\sigma}$ is defined in terms of the spin angular momentum S as follows:

$$S = \begin{cases} (\hbar/2)\underset{\sim}{\sigma} & \text{proton} \\ \hbar\underset{\sim}{\sigma} & \text{deuteron} \end{cases}$$

Finally, $\underset{\sim}{r}-\underset{\sim}{r}'$ is the relative separation of the interacting particles describing a non-local potential $U(\underset{\sim}{r},\underset{\sim}{r}')$ represented by the expression

$$U(\underset{\sim}{r}-\underset{\sim}{r}') = U[(\underset{\sim}{r}-\underset{\sim}{r}')/2]\exp[-\{(\underset{\sim}{r}-\underset{\sim}{r}')/\beta\}^2]/\pi^{3/2}\beta^3$$

Since β is a measure of the range of non-locality, in the low energy region, $\beta \to 0$ then $U(\underset{\sim}{r},\underset{\sim}{r}') \to U(\underset{\sim}{r})$ becomes a local potential (H071).

The above non-local potential was calculated from a nucleon-nuclear interaction. The optical model takes into account all interactions between the incident particle and the target nucleons.

In this work we consider the elastic scattering of incident particles from a target nucleus. In the local approximation, the momentum transferred between the collisions with the target nucleons must be small in order that the internal state of the nucleus remains unchanged. This implies that long range collisions or Coulomb scattering may contribute strongly to forward angle scattering.

There are certain ambiguities in the optical parameters occurring in the analysis of the experimental data. The procedure is to begin with acceptable parameters and then iterate to optimize a fit to the measured data. The iteration is carried out until the discrepancy between the experimental and the theoretical cross-sections is a minimum. However, there is the danger of obtaining an unphysical solution for the above method. Such ambiguities are most generally associated with:

a) the incorrect potential form factor;

b) Vr^n, where n=1, 2, or 3 or Wa_w = const.;

c) many potential depths give comparable fits to the data; and

d) over-all normalization error for the experimental data.

2.3 Scattering Amplitudes

For a nucleon-nucleus interaction, the incoming and outgoing particles of spin components m and m' satisfy the Schrödinger equation,

$$H\Psi_m = E_{CM}\ \Psi_m, \qquad (2.3\text{-}1)$$

and the solution (Ho 71) may be written asymptotically as

$$\Psi_{m\ r \tilde{\to} \infty} [1 + \eta^2/ik(r-z)] * \exp[i(kz + \eta \ell n\ k(r-z))]\ \chi_s^m + \sum_{m'} f_{mm'}(\theta)(1/kr)\ \exp[i(kr-\eta \ell n\ 2kr)]\ \chi_s^{m'} \qquad (2.3\text{-}2)$$

The first term is a pure Coulomb wave with $\eta = Z_p Z_t e^2/\hbar k$ and the second term is an outgoing spherical wave with $f_{mm'}(\theta)$, the scattering amplitude term for an incoming particle scattered through a centre of mass angle θ; while χ_s^m and $\chi_s^{m'}$ are the spin-wave functions for the incoming and outgoing particles.

A partial wave expansion for Ψ_m in the Schrödinger equation (Ho71) with total anglar momentum J and orbital angular momentum L is written asymptotically as

$$\Psi_{m\ r \tilde{\to} \infty} \sum A_{JLm}\ (1/kr)\ R_{JL}\ F_{JLm} \qquad (2.3\text{-}3)$$

where the spin-angle functions are the F_{JLM} terms further expressed as

$$F_{JLm} = \sum (LS\ ;m-m'\ m'|Jm) Y_L^{m-m'}(\theta,0)\chi_s^{m'} \qquad (2.3\text{-}4)$$

The Clebsch-Gordan (or Wigner) coefficient terms, (LS; m-m' m'|Jm) are often referred to as vector-addition coefficients.

The expansion coefficient terms, A_{JLm} are

$$A_{JLm} = i^{L} [4\pi(2L + 1)]^{\frac{1}{2}} \quad (LS; 0m|Jm), \tag{2.3-5}$$

while the radial wave functions, $R_{JL}(r)$ satisfy the equation

$$[d^2/dr^2 - L(L + 1)/r^2 + k^2 - 2\mu/\hbar^2 * < JL|U(r)|JL)>] R_{JL}(r) = 0 \tag{2.3-6}$$

where U(r) is the optical potential discussed in Section 2.1. The solution for the above equation is given in terms of the Coulomb functions F_L and G_L,

$$R_{JL}(r) \underset{r \to \infty}{\sim} e^{i\sigma_L} [F_L(r) + \alpha_L^J (G_L(r) + iF_L(r))] \tag{2.3-7}$$

and the absolute Coulomb phase shifts, σ_L defined by the following relation,

$$\exp(2i\sigma_L) = \Gamma(1 + L + i\eta) / \Gamma(1 + L - i\eta) \tag{2.3-8}$$

and finally the nuclear scattering amplitudes, α_i^J further expressed in terms of the nuclear phase shifts δ_L^J, or

$$\alpha_L^J = (1/2i)\exp(2i\delta_L^J) - 1 \tag{2.3-9}$$

Asymptotically, the Coulomb functions F_L and G_L are defined by

$$\begin{Bmatrix} F_L \\ G_L \end{Bmatrix} \xrightarrow[r \to \infty]{} \begin{Bmatrix} \sin \\ \cos \end{Bmatrix} (kr-\eta \ell n\ 2kr - L\pi/2 + \sigma_L) \qquad (2.3\text{-}10)$$

Thus; rewriting equation (2.3-3) as a Coulomb wave function and the partial wave expansion for the outgoing sherical wave,

$$\Psi_m \underset{r \to \infty}{\sim} \Psi_m^{\text{Coulomb}} + \sum_{JL} [4\pi(2L+1)^{\frac{1}{2}} (LS;0m|Jm) * (1/kr)\, \alpha_L^J \exp[i(kr-\eta \ell n\ 2kr)] * \exp(2i\sigma_L) \sum_{m'} (LS;\ m-m'\ m'|Jm) * Y_L^{m-m'}(\theta,0)\ \chi_s^{m'} \qquad (2.3\text{-}11)$$

and rewriting equation (2.2.2) in a similar manner, one obtains

$$\Psi_m \underset{r \to \infty}{\sim} \Psi_m^{\text{coulomb}} + \sum_{m} (f_{mm'}(\theta) - f_c(\theta)\delta_{mm'}) * (1/kr)\exp[i(kr-\eta \ell n\ 2\ kr)]\ \chi_s^{m'} \qquad (2.3\text{-}12)$$

where fc is the Coulomb scattering amplitude

$$f_c(\theta) = -(\eta/2)\csc^2(\theta/2)\exp(-2i\eta \ell n\ \sin(\theta/2) + 2i\sigma_o) \qquad (2.3\text{-}13)$$

Equating co-efficients from equations (2.3-10, 12), one obtains a partial wave expansion for the nuclear scattering amplitude

$$f_{mm'}(\theta) = f_c(\theta)\,\delta_{mm'} + \sum_{JL}[4\pi(2L+1)]^{1/2} *\exp(2i\sigma_L)\alpha_L^J\,(LS;om|Jm)(LS;m-m'm'|Jm)Y_L^{m-m'}(\theta,0)$$

(2.3-14)

For the elastic scattering of spin ½ or 1 particles from a spin 0 nucleus, the expansions for $f_{mm'}(\theta)$ are given in Appendix A.

The differential cross section for incident particles is given in terms of the scattering amplitude $f_{mm'}(\theta)$

$$\sigma(\theta) = [1/k^2(2S+1)]\ \mathrm{Tr}\ \{f(\theta)f^{\ddagger}(\theta)\}$$
$$= [1/k^2(2S+1)] \sum_{mm'} |f_{m'm}(\theta)|^2$$

(2.3-15)

Rewriting $\sigma(\theta)$ in terms of the scattering amplitudes $f_{mm'}(\theta)$ found in Appendix A for spins ½ and 1 respectfully,

S = ½

$$\sigma(\theta) = (1/k^2)\ \{|f_{\frac{1}{2}\frac{1}{2}}|^2 + |f_{\frac{1}{2}-\frac{1}{2}}|^2\}$$

(2.3-16a)

S = 1

$$\sigma(\theta) = (1/3k^2)\ \{|f_{00}|^2 + 2(|f_{11}|^2 + |f_{10}|^2 + |f_{01}|^2 + |f_{1-1}|^2)\}$$

(2.3-16b)

CHAPTER 3

EXPERIMENTAL

3.1 Experimental setup

In the magpak experimental area at the Nuclear Research Centre, the incident proton or deuteron beam from the Van de Graaff accelerator was collimated by two adjustable low-background beam-defining slits upstream and an antiscattering slit (Ro69) located at the scattering chamber. (fig. 3.1) Measurements were taken in an 18-inch diameter scattering chamber, where inside were four surface-barrier detectors, that is, three moveable detectors at 10 degree intervals, located at a distance of 8 inches from the centre while the fourth detector, 9 inches from the centre and stationary at 30 degrees to the beam, used as a monitor. An important feature of the chamber allowed the detectors to be moved in one degree steps or less. In front of each detector, circular collimators of different solid angles were placed depending on the count rate. By observing 2.5 MeV protons elastically scattered from ^{40}Ca the relative solid angles of the collimators were measured. The output analog pulses from each of the detectors went through a preamp-amp-ADC-DDP516 configuration for real-time data acquisition and finally into a XDS940 computer for off-line data analysis.

The targets were made by evaporating approximately 20 $\mu g/cm^2$ of natural calcium metal (96.6% ^{40}Ca) onto a carbon-formvar backing. The thin layer of carbon was used to dissipate heat from the beam while the formvar was used for mechanical strength of the target. Because of the chemical properties of calcium, that is, oxidation of the metal,

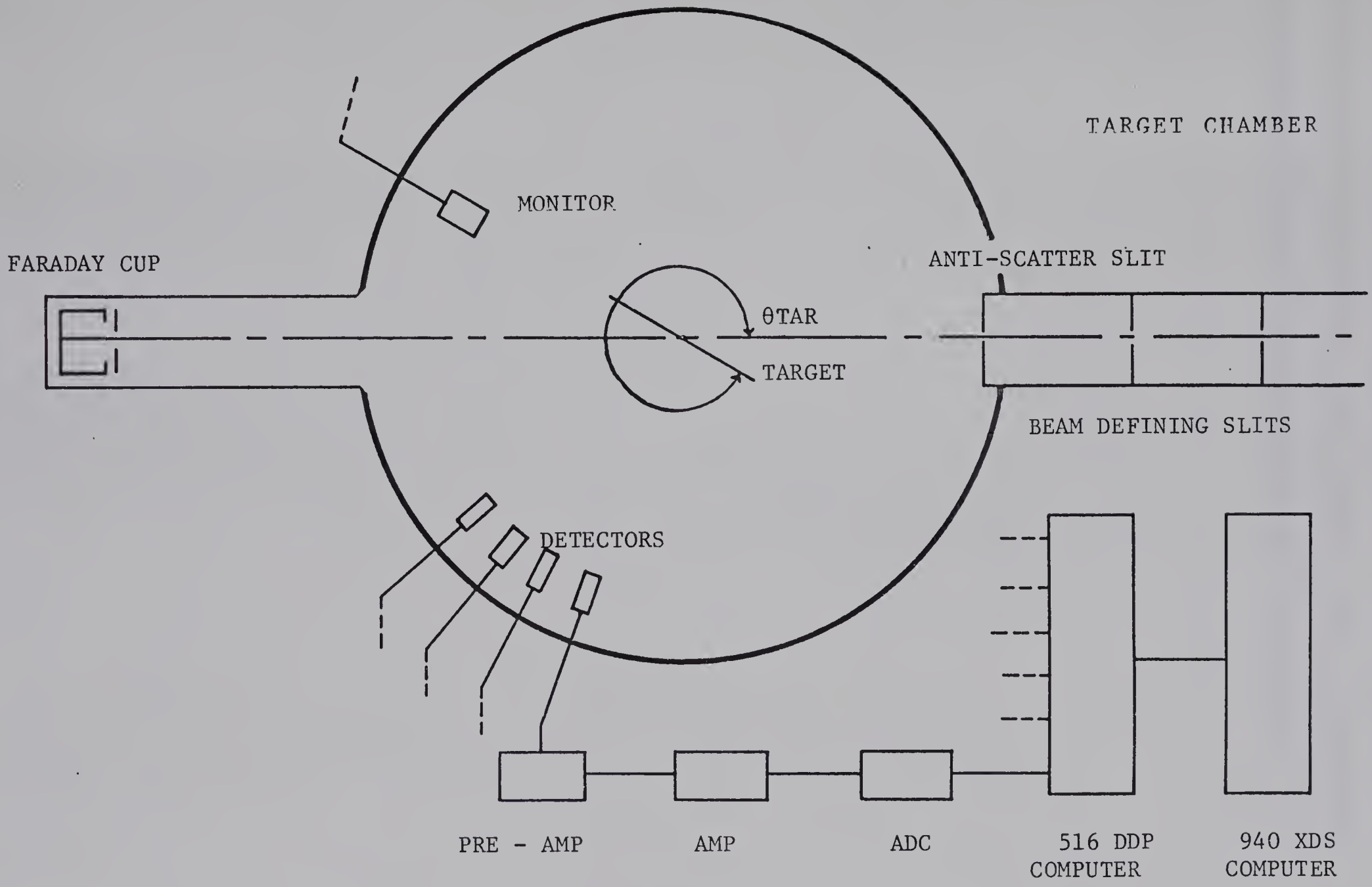

Fig. 3.1 Schematic of Experimental Arrangement

the problem of eliminating oxygen completely was impossible with the present evaporating system-target chamber method since air was always present at some stage of the preparation.

3.2 Relative cross-sections

Cross-sectional data was measured in five degree steps or less, in the angular distribution range, 7-160 degrees, and many of the experimental runs were repeated to obtain statistical results with the following corrections:

i) background and multiple scattering

The probability that n events will occur in any one channel of an ADC energy spectrum is a Poisson distribution. If the number of events or counts under a typical elastic peak in the energy spectrum is large, then the approximation to a gaussian function,

$$P(x) = (A/\ 2\sigma)\exp[-(\tfrac{1}{2})((x-\overline{x})/\sigma)^2] \qquad (3.2\text{-}1)$$

with parameters A for the area, σ for the standard deviation in A and $\overline{x}$ is the c.m. energy centroid; is a standard least squares peak fitting procedure. The independent weights w_i assigned in the equation below for the minimizing function Δ,

$$\Delta = \sum_i w_i[P_i^{TH}(x)-P_i^{exp}(x)] \qquad (3.2\text{-}2)$$

are the square root of the number of counts for each channel. The peak fitting program has the following features:

a) background subtraction

b) separation of ^{12}C and ^{16}O peaks from ^{40}Ca

c) separation of multiple scattering events (i.e. in the forward angle region) which produce a skew gaussian

d) evaluation of a physical statistical error for the area under the peak.

ii) dead-time corrections for the ADC's.

If the logic gate is open, an ADC will accept a random pulse from a detector and become busy, i.e. will not accept any more pulses. The analog pulse is converted to a digital pulse. The gate is closed and the ADC is ready for the computer. When the information is dumped, the ADC is reset and the gate is open to accept another random pulse.

Since the count rate varies approximately as $1/\sin^4(\theta/2)$, the dead time for the forward angles may be greater than at the backward angles where the count rate is not large.

The relative peak sum was normalized to the monitor located 30 degrees to the beam with the following correction.

$$\text{Psum} = \text{Mav} \ \frac{\text{Dsum/DLT}}{\text{Msum/MLT}} \qquad (3.2\text{-}3)$$

where the following symbols are defined below:

Psum - relative peak sum,

Dsum - detector peak sum,

Msum - monitor peak sum,

DLT - detector livetime,

MLT - monitor livetime,

Mav - average monitor sum.

iii) Solid angle corrections

Since the count rate varies approximately as $1/\sin^4(\theta/2)$, collimators of different solid angle were placed in front of each detector. Normalization was done using 2.5 MeV protons elastically scattered from ^{40}Ca at 30 degrees.

iv) target thickness, including deterioration and beam stability using low energy protons.

v) target-angle corrections at 90 degrees.

The target was at 330 degrees to the beam for the forward angles and changed to 30 degrees for the backward angles.

vi) conversion of the lab system to the centre of mass system

$$\left.\frac{d\sigma(\theta)}{d\Omega}\right|_{cm} = \frac{m_p m_t\left[(m_t/m_p)^2 - \sin^2\Psi\right]^{\frac{1}{2}}}{(m_p + m_t)^2 (E_1/E_{inc})} \left.\frac{d\sigma(\Psi)}{d\Omega}\right|_{Lab} \qquad (3.2\text{-}4)$$

where ψ is the laboratory angle and E_{inc} is the incident particle energy, while E_1 is the energy of the particle scattered from a target nucleus. The other parameters are defined in Section 2.1.

vii) since the experimental runs were short, i.e. 5-8 minutes, many of the runs were repeated to obtain good statistics. Defining $\bar{x}$ as the mean peak sum

area,

$$\bar{x} = \sum_i w_i x_i / \sum_i w_i \quad , \; i=1,N \tag{3.2-4}$$

and the weight w_i is written as

$$w_i = 1/\Delta x_i^2 \tag{3.2-5}$$

is related to the error in the peak sum. From the definition of chi-squared

$$\chi^2 = \sum_i w_i (\bar{x} - x_i)^2 \, , \tag{3.2-6}$$

therefore the error in Δx is

$$\Delta \bar{x} = \{(1/\Sigma w_i)(\chi^2/(n-1))\}^{1/2} \tag{3.2-7}$$

where n is the number of degrees of freedom.

3.3 Absolute Cross Sections

From the elastic scattering of low-energy protons in the 2.5 - 3.5 MeV range, the absolute cross sections should be nearly Rutherford in the forward-angle region and the relative-to-absolute conversion factor should not be difficult to obtain for a target nucleus such as calcium. However, for the light nuclei, carbon and oxygen, nuclear contributions (BL65, HA62 and RE56) provide difficulties in finding satisfactory conversion factors; as a result, the absolute cross-section error bars are large. To show the above behavior, theoretical curves are generated (figs. 3.1 - 3.2) using an optical-model search program on the proton experimental data starting with the initial parameters in Table 3.1 below.

Table 3.1 Initial Parameters for ^{12}C and ^{16}O Proton Data

V (MeV)	R_0 (fm)	A_0 (fm)	W_D (MeV)	R_W (fm)	A_W (fm)	V_{SO} (MeV)	R_{SO} (fm)	A_{SO} (fm)
50.0	1.25	0.65	8.5	1.25	0.52	9.0	1.25	0.64

Searching only on the potentials W_D and V_{SO} with the computer program SNOOPY* gave a nonphysical range of values for both. W_D was between 7.21 - 17.23 MeV and the range of the spin orbit potential V_{SO} was from 1.75 - 35.28 MeV. The geometrical potential parameters were calculated and gave no improvement to the fit. The nonphysical potential parameters calculated by the search program SNOOPY were due to

i) few experimental data points, all of which were in the forward angle-region;

ii) the resonance structure present for both ^{12}C and ^{16}O nuclei (BL65, HA62 and RE56) in the low-energy proton spectrum region; and finally

iii) the optical model breaks down below 5.0 MeV.

The only reasonable parameters to use for calculations of the optical model are found in Table 3.1, obtained from references HO71 and PE63. From figures 3.1 and 3.2, one finds the relative-to-absolute conversion factors are difficult to acquire with any degree of accuracy; therefore, the absolute cross sections for ^{12}C and ^{16}O experimental data were obtained from normalizations to 5.0 MeV deuteron data found elsewhere in the literature (DA70 and OH63).

---

* Obtained from W. Haeberli, University of Wisconsin, Madison, Wisconsin.

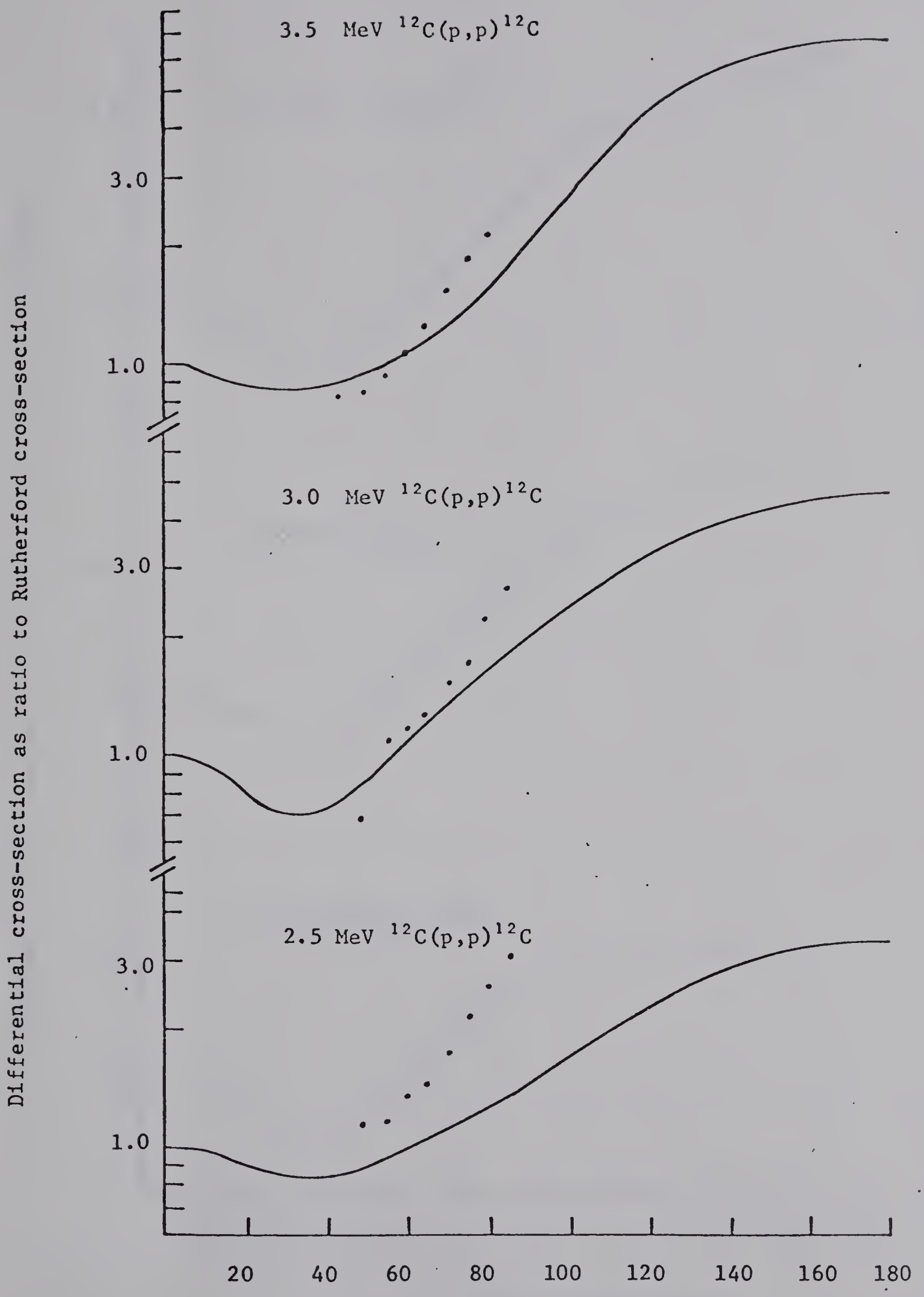

Figure 3.1 2.5, 3.0 and 3.5 MeV $^{12}C(p,p)^{12}C$

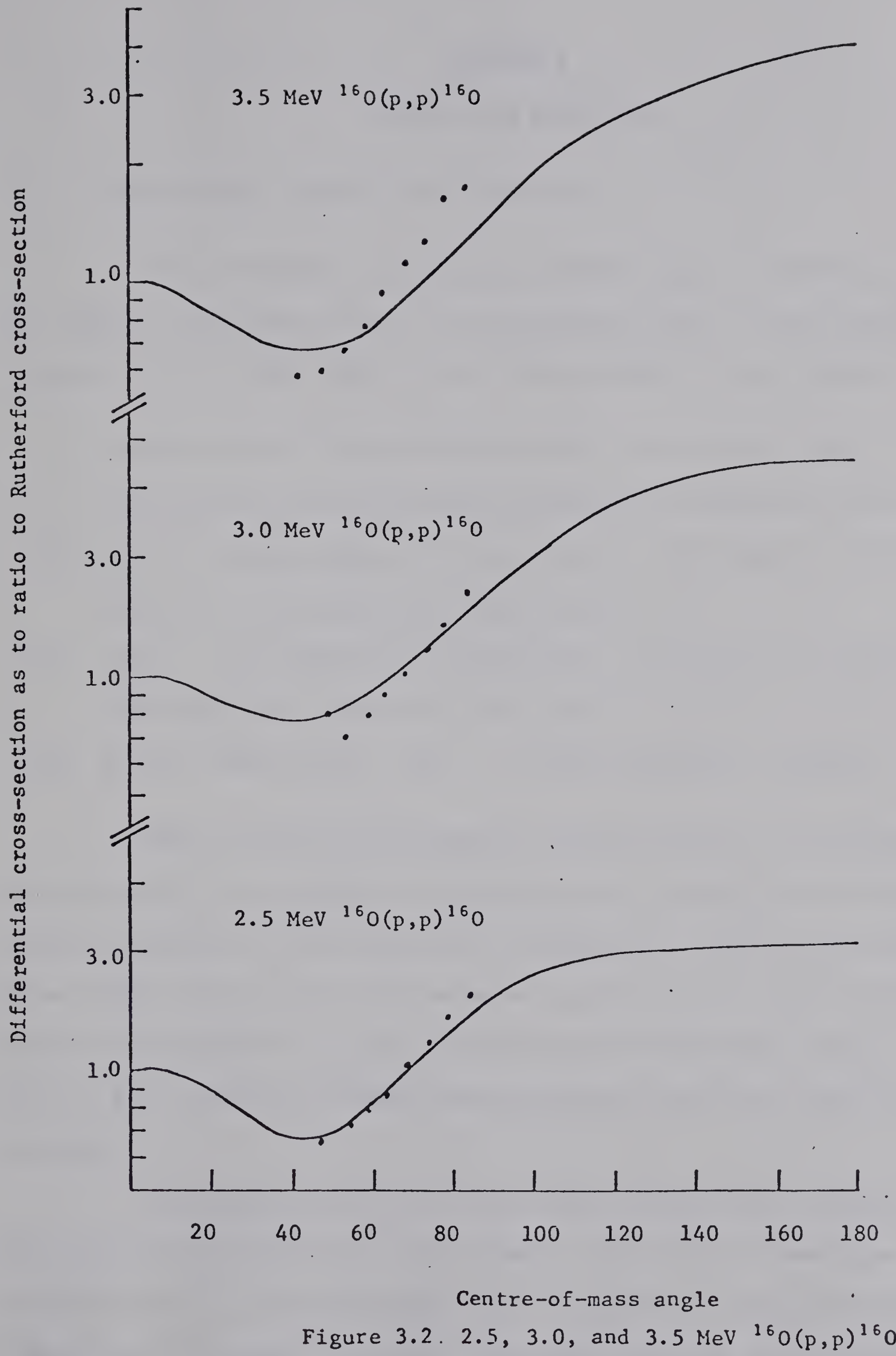

Figure 3.2. 2.5, 3.0, and 3.5 MeV $^{16}O(p,p)^{16}O$

CHAPTER 4

RESULTS AND DISCUSSION

4.1 Optical-model Analysis of 5.0 MeV Data.

From the elastic cross-section measurements, an attempt to find the optical potentials that fit the experimental data was made using a computer program called SNOOPY. The fitting procedure is as follows:

i) optimize fits to the experimental data starting first with the potentials V, W_D, and V_{SO} while leaving the geometrical parameters fixed;

ii) use the maximum number of partial waves so the nuclear contributions from all L values are taken into account;

iii) vary the geometrical parameters R_0, A_0, R_W, A_W, R_{SO} and A_{SO} each separately leaving the rest fixed;

iv) finally simultaneous vary all the parameters together.

From i) and iii), the general fitting behavior of the parameters may be studied, i.e. W_D fits the backward angles and V SO fits the dip around 90 degrees. Searching on all the paramets in iv) at once should give little change in both the parameter and chi-squared values. Using only a few L-values in ii), say computed from the classical result $\vec{L} = \vec{r} \times \vec{p}$, one finds sometimes the parameters varied gave nonphysical results.

The parameters may not be physically correct even though they fit the cross-sectional data. For example, if there is a resonance structure present one would expect rapid variation of the optical-model parameters with energy. Therefore the proper choice is to use parameters

changing smoothly with energy. One should also remember that the optical model description for elastic scattering gives only the asymptotic behavior of the wave functions, but indicates little about what goes on inside the nucleus.

The initial parameters searched for the elastic scattering of 5.0 MeV deuterons on ^{12}C, ^{16}O and ^{40}Ca nuclei are shown in Table 4.1 below.

Table 4.1 INITIAL OPTICAL-MODEL PARAMETERS

V (MeV)	R_0 (fm)	A_0 (fm)	W_D (MeV)	R_W (fm)	A_W (fm)	V_{SO} (MeV)	R_{SO} (fm)	A_{SO} (fm)
100	1.05	0.85	8.5	1.66	0.53	9.0	0.9	0.65

The function χ^2, defined as

$$\chi^2 = (1/N)\sum_{i=1}^{N} [(d\sigma(\theta)d\Omega)_{TH} - (d\sigma(\theta)/d\Omega)_{EXP})/(\Delta d\sigma(\theta)/d\Omega)]^2$$

was used to compare the fits in terms of the optical-model parameters. Here, $(d\sigma(\theta)/d\Omega)_{TH}$ and $(d\sigma(\theta)/d\Omega)_{EXP}$ are the calculated and experimental absolute cross sections, respectively, for the centre-of-mass angle θ_i while the weight assigned, $(\Delta d\sigma(\theta)/d\Omega)_{EXP}$ is the experimental error. The above expression for χ^2 assumes the errors are uncorrelated for each data point. However, errors from the elastic scattering events

come not only from the statistics of the number of points or area in the elastic peak, or the number of repeated runs, but also from measurements of target thickness, solid angle, dead-time corrections and so forth which may or may not be correlated with angle θ.

The present analysis uses an automatic parameter search routine which minimizes chi-square with respect to any desired number of parameters. The numerical value of χ^2 obtained does not give a very definite idea of the fit while the use of χ^2 as a measure of goodness of fit is more meaningful. Frequently, the automatic search ends in a secondary minimum or valley of the χ^2 surface in parameter space, particularly when the number of parameters varied is large or when only a few partial waves are used.

4.2 5.0 MeV $^{12}C(d,d)^{12}C$ and $^{16}O(d,d)^{16}O$.

The theoretical curves in figures 4.1 - 4.2 are generated from the optical model parameters shown in Tables 4-2 and 4.3 below.

Table 4.2 OPTICAL MODEL PARAMETERS FOR 5.0 MeV $^{12}C(d,d)^{12}C$

V (MeV)	R_0 (fm)	A_0 (fm)	W_D (MeV)	R_W (fm)	A_W (fm)	V_{SO} (MeV)	R_{SO} (fm)	A_{SO} (fm)
104.96	1.136	0.85	5.39	1.612	0.53	8.89	0.792	0.64

Table 4.3 OPTICAL MODEL PARAMETERS FOR 5.0 MeV $^{16}O(d,d)^{16}O$

V (MeV)	R_0 (fm)	A_0 (fm)	W_D (MeV)	R_W (fm)	A_W (fm)	V_{SO} (MeV)	R_{SO} (fm)	A_{SO} (fm)
102.35	1.046	0.85	4.81	1.992	0.53	11.99	0.70	0.64

The theoretical optical dip about 20 degrees found in figures 4.1 - 4.2 is important since the deviation from Rutherford scattering for both ^{12}C and ^{16}O nuclei at 5.0 MeV is shown here. For all sets of parameters searched on, even varying the number of partial waves one finds that the nuclear part of the scattering amplitude dominates; in other words, the dip was always present. Since,from the energy spectrum, the centre of mass of both ^{12}C and ^{16}O, elastic peaks shifts into ^{40}Ca, it becomes rather difficult to analyse for the nuclear contributions experimentally.

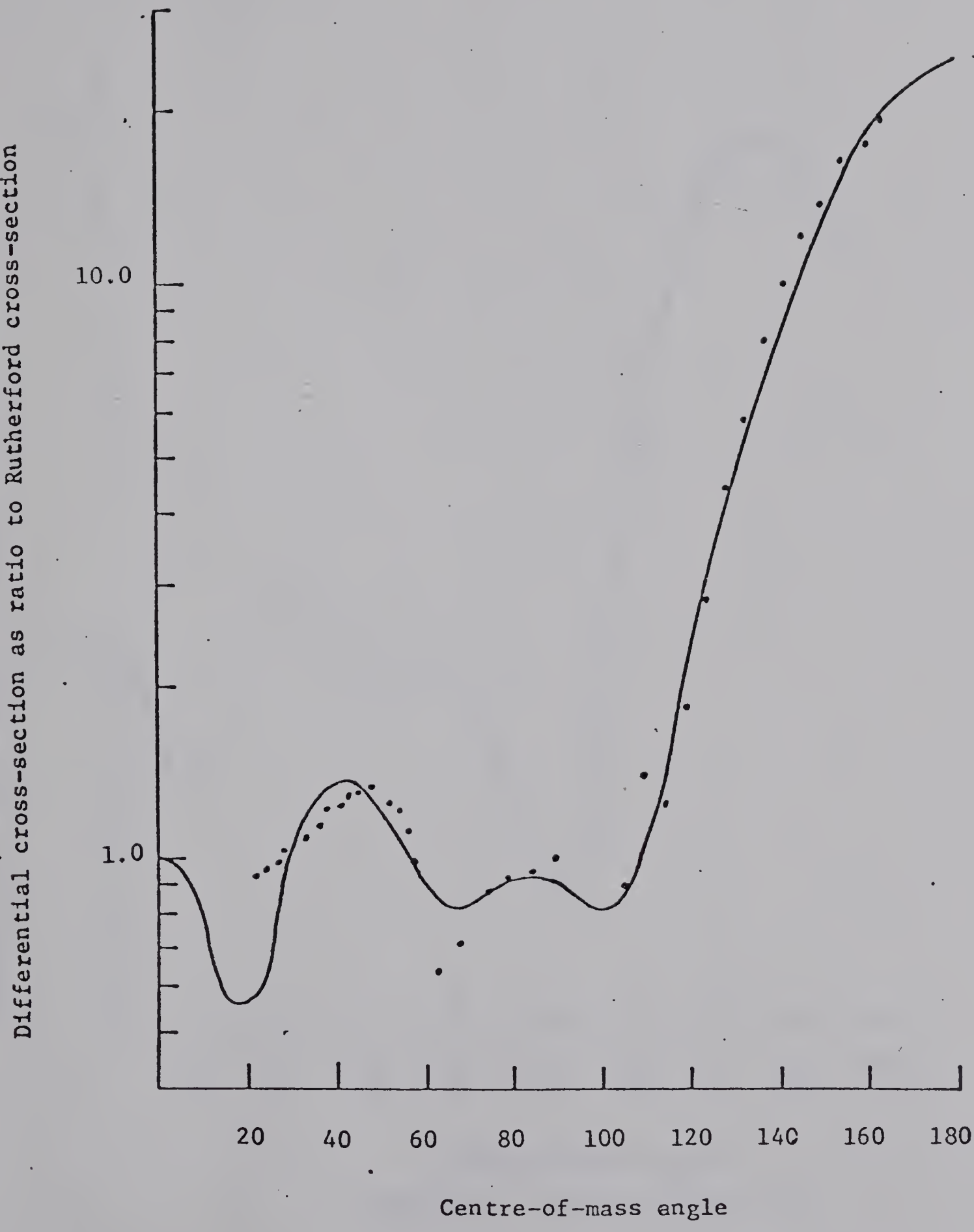

Figure 4.1 5.0 MeV $^{12}C(d,d)^{12}C$

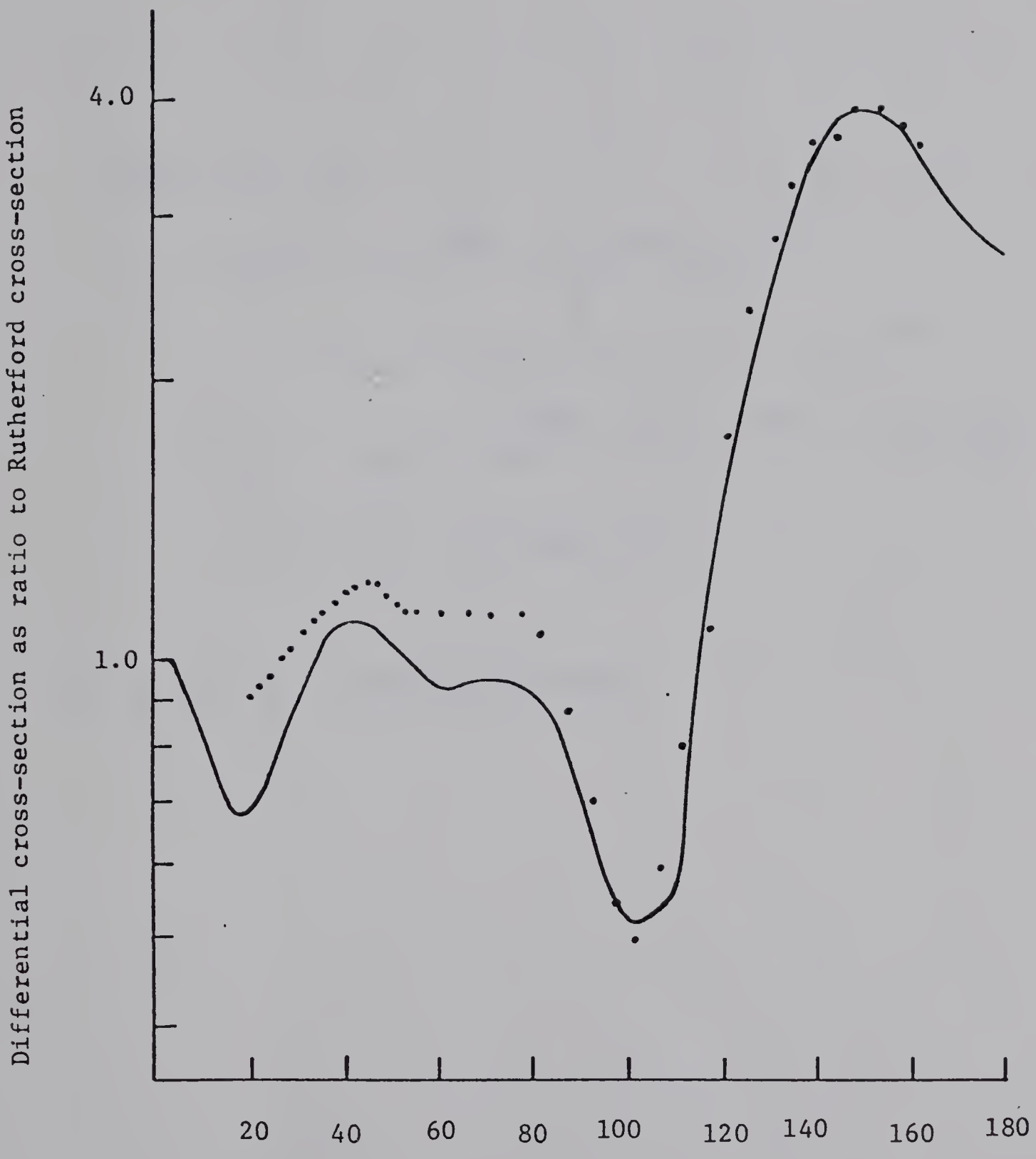

Figure 4.2 5.0 MeV $^{16}O(d,d)^{16}O$

Even if one could predict the nuclear part of the scattering amplitude, there would still be the interference term between the nuclear and Coulomb parts shown below

$$
\begin{aligned}
|f|^2 &= |f_N + f_c|^2 \\
&= |f_N| e^{i\phi_N} |f_N| e^{-i\phi_N} + |f_N| e^{i\phi_N} |f_c| e^{-i\phi_c} \\
&\quad + |f_c| e^{i\phi_c} |f_N| e^{-i\phi_N} + |f_c| e^{-i\phi_c} |f_c| e^{+i\phi_c} \\
&= |f_N|^2 + |f_N|\,|f_c|\,(e^{i(\phi_N - \phi_c)} + e^{-i(\phi_N - \phi_c)}) + |f_c|^2 \\
&= |f_N|^2 + 2|f_N|\,|f_c| \cos(\phi_N - \phi_c)
\end{aligned}
$$

where $\phi_N - \phi_c$ is the interference angle.

4.3 5.0 MeV ^{40}Ca (d,d) ^{40}Ca.

The results from the optical model calculations are shown in fig. 4.3 and in the table below.

Table 4.4 OPTICAL MODEL PARAMETERS FOR 5.0 MeV $^{40}Ca(d,d)^{40}Ca$

V (MeV)	R_0 (fm)	A_0 (fm)	W_D (MeV)	R_W (fm)	A_W (fm)	V_{SO} (MeV)	R_{SO} (fm)	A_{SO} (fm)
103.35	1.053	0.934	9.82	0.655	0.511	8.5	1.302	0.725

The sensitivity of the optical model parameters particularly to small deviations from Rutherford around 15 degrees in figure 4.3 is important. The physical potential parameters obtained from the optical model calculations were not sensitive in the above forward angle region. Using only the experimental data points less than 90 degrees again predicted the same behavior.

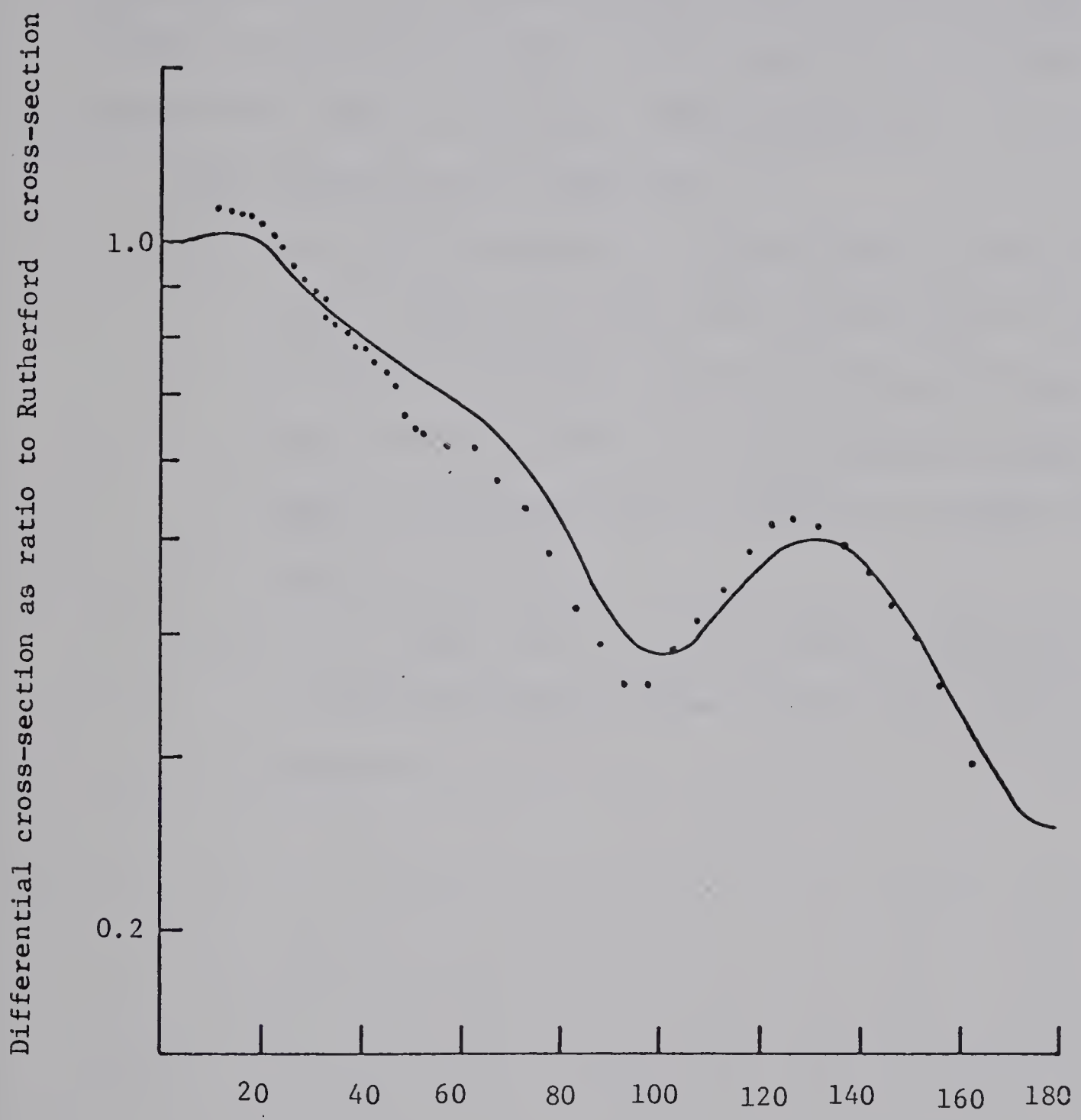

Figure 4.3 5.0 MeV $^{40}Ca(d,d)^{40}Ca$

4.4 Summary and Conclusions

From the analysis of the present data it may be concluded that the elastic scattering of 5.0 MeV deuterons on ^{40}Ca is not pure Rutherford scattering in behavior (nuclear bump around 15 degrees). Also solving the problem of separating the other elastic peaks from one another in the forward angle region represents a problem unsolved.

Two proposals may be suggested:

i) Run 5.0 MeV deuterons on a carbon backing at the forward-angular region. From the elastic scattering of 2.0 MeV protons on ^{12}C, the approximate amount of ^{16}O may be found. For some angles where the elastic peaks are separate compare with the angular distribution results of ^{40}Ca on a carbon backing for oxygen contamination.

ii) Make an oxygen gas cell for the target chamber and obtain an angular distribution from 2.0 MeV protons and 5.0 MeV deuterons.

REFERENCES

BL 65 R.A. BLUE and W. HAEBERLI, Phys. Rev. 137 (1965) B284.

DA 70 N.E. DAVISON, W.K. DAWSON, G. ROY and W.J. McDONALD, Can. J. Phys., 48 (1970) 2235.

HA 62 R.W. HARRIS, G.C. PHILLIPS and C.M. JONES, Nucl. Phys. 38 (1962) 259.

HO 71 P.E. HODGSON, Nuclear Reactions and Nuclear Structure, Oxford Clarendon Press, (1971).

KE 72 M.P. KEATING and J.G. WILLS, Phys. Rev. C5 (1972) 1572.

OH 63 G.G. OHLSEN and R.E. SHAMU, Nucl. Phys. 45 (1963) 523.

PE 63 F.G. PEREY, Phys. Rev. 131 (1963) 745.

RE 56 C.W. REICH, G.C. PHILLIPS and J.L. RUSSELL, Jr., Phys. Rev. 104 (1956) 143.

RO 69 G. ROY and N. RIEBEEK, Nucl. Instr. and Meth., 71 (1969) 234.

SC 69 P. SCHWANDT and W. HAEBERLI, Nucl. Phys., A123 (1969) 401.

APPENDIX I

Nuclear Scattering Amplitudes for Spin ½ and 1 Particles

From Section 2.3, a partial wave expansion of the scattering amplitude was obtained for the $f_{mm'}(\theta)$ term in equation 2.3-14. The explicit expressions for $f_{mm'}(\theta)$ are now given below.

i) $\underline{S = \frac{1}{2}}$

$$f_{\frac{1}{2}\frac{1}{2}}(\theta) = f_c(\theta) + \sum_L e^{2i\sigma_L}\left[(L+1)\alpha_L^{L+\frac{1}{2}} + L\alpha_L^{L-\frac{1}{2}}\right]P_L(\cos\theta)$$

$$f_{\frac{1}{2}-\frac{1}{2}}(\theta) = \sum_L e^{2i\sigma_L}\left[\alpha_L^{L+\frac{1}{2}} - \alpha_L^{L-\frac{1}{2}}\right]P_L^1(\cos\theta)$$

ii) $\underline{S = 1}$

$$f_{00}(\theta) = f_c(\theta) + \sum_L e^{2i\sigma_L}\left[(L+1)\alpha_L^{L+1} + L\alpha_L^{L-1}\right]P_L(\cos\theta)$$

$$f_{11}(\theta) = f_c(\theta) + \sum_L e^{2i\sigma_L}(\tfrac{1}{2})\left[(L+2)\alpha_L^{L+1} + (2L+1)\alpha_L^{L} + (L-1)\alpha_L^{L-1}\right]P_L(\cos\theta)$$

$$f_{10}(\theta) = \sum_L e^{2i\sigma_L}(1/\sqrt{2})\left[\alpha_L^{L+1} - \alpha_L^{L-1}\right]P_L^1(\cos\theta)$$

$$f_{01}(\theta) = \sum_L e^{2i\sigma_L}[1/\sqrt{2}\ L(L+1)][-L(L+2)\alpha_L^{L+1}$$

$$+(2L+1)\alpha_L^L + (L+1)(L-1)\alpha_L^{L-1}]\ P_L^1(\cos\ \theta)$$

$$f_{1-1}(\theta) = \sum_L e^{2i\sigma_L}\ [\tfrac{1}{2}L(L+1)][L\alpha_L^{L+1} - (2L+1)\alpha_L^L$$

$$+ (L+1)\alpha_L^{L-1}]\ P_L^2(\cos\ \theta)$$